DOI: 10.1002/ejic.201100395

Dye-Sensitised Solar Cells Based on Large-Pore Mesoporous TiO_2 with Controllable Pore Diameters

Kai Pan,[a] Wei Zhou,[a] Guohui Tian,[a] Qingjiang Pan,[a] Chungui Tian,[a] Tengfeng Xie,[b] Youzhen Dong,[a] Dejun Wang,[b] and Honggang Fu*[a]

Keywords: Solar cells / Mesoporous materials / Nanoparticles / Photovoltage transient / Interfacial electron transfer / Electrolyte percolation / Adsorption

Mesoporous TiO_2 (meso-TiO_2) is a promising photoelectrical nanomaterial for high dye-sensitised solar cell (DSSC) performance, because its nanochannels offer a large internal surface area to allow for more dye adsorption. The interconnected grains facilitate rapid electron transport both within the meso-TiO_2 film and at the film electrode dye/redox shuttle electrolyte interfaces. In this work, a series of DSSCs has been fabricated on the basis of meso-TiO_2 with large controllable pore sizes (6.5, 8.2 and 11.0 nm). It was found that the DSSC with the 8.2 nm meso-TiO_2 photoelectrode has the highest photoelectrical conversion efficiency, which is higher than that of the conventional P25 nanoparticulate DSSC under the same conditions. The measurements of the N_2 sorption isotherms and the photovoltage transient demonstrates that such improved efficiency can be ascribed to the larger surface area and the fastest interfacial charge transfer. Meanwhile, the effect of different pore sizes on the photoelectrical conversion efficiency has been systematically investigated, and a possible model for the efficient electrolyte percolation in the dye-sensitised mesoporous photoelectrode has been proposed.

Introduction

Since the outstanding work of M. Grätzel in 1991, dye-sensitised solar cells (DSSCs) have become a possible economical alternative to conventional solar energy cells.[1–4] Generally, DSSCs are composed of a nanocrystalline semiconductor oxide photoelectrode, a dye sensitiser, a redox shuttle and a counter electrode.[5,6] Under illumination, an electron is injected into the conduction band of the semiconductor photoelectrode from the excited state of the sensitiser. The oxidised dye can be recovered by means of a suitable redox shuttle. The diffusion of the oxidised shuttle to the counter electrode completes the circuit.[7–9] In principle, fast photoelectron transfer and slow recombination will bring about a higher photoelectrical conversion efficiency (η). It has been established that there are a number of factors determining the overall conversion efficiency. Among them, the structural and physical properties of the nanocrystalline semiconductor oxide are predominant.[10]

A nanoporous TiO_2 (np-TiO_2) nanoparticulate film is an excellent starting photoelectrode for DSSCs due to its facile fabrication and low cost.[11–13] However, the vast majority of the nanopores in the films are derived from the intercrystalline voids rather than regular and integrated pores. Some of the internal pores are in the micrometer range, which prevents adsorbtion of the sensitisers or access to the electrolyte.[14] Therefore, some strategies in recent years have been attempted to optimise the structures of photoelectrodes to increase the η value of DSSCs. One of them was to replace the np-TiO_2 with bead-like TiO_2, 1D nanomaterials, and so on.[15–17] Another promising strategy was to apply mesoporous TiO_2 (meso-TiO_2) as a DSSC photoelectrode, because the mesostructure within the meso-TiO_2 offers a large internal surface area, which allows for more dye adsorption and thus more efficient light absorption compared with np-TiO_2. Furthermore, these porous films with interconnected grains facilitate rapid electron transport within the meso-TiO_2 film and highly efficient charge transfer at interfaces of the film electrode dye/redox shuttle electrolyte.[18] Hence, meso-TiO_2 is an ideal candidate photoelectrode nanomaterial for DSSCs with a high conversion efficiency.

DSSCs with meso-TiO_2 photoelectrodes have been an active subject around the world.[19–23] I. Kartini et al. applied mesoporous TiO_2 with a pore diameter of 7.7 nm to fabricate DSSCs, which achieved an η value of 5.05%.[19] Mesoporous TiO_2 with a pore diameter of 6.2 nm was prepared by K. Hou et al. using surfactant P123 as a template, and the corresponding DSSCs had an η value of 5.31%.[20] M. Wei et al. fabricated DSSCs with a 6.1 nm mesoporous

[a] Key Laboratory of Functional Inorganic Material Chemistry, Ministry of Education, School of Chemistry and Materials Science, Heilongjiang University,
Harbin 150080, People's Republic of China
Fax: +86-451-8667-3647
E-mail: fuhg@vip.sina.com
[b] College of Chemistry, Jilin University,
Changchun 130012, People's Republic of China

Supporting information for this article is available on the WWW under http://dx.doi.org/10.1002/ejic.201100395.

TiO_2 photoelectrode. The relationship between the photovoltaic performance and the physicochemical properties of mesoporous TiO_2, such as surface area and pore diameter, was investigated. It was found that the mesopore structure significantly affected the photovoltaic performances.[21] All of the above work is interesting and valuable, but these researches mainly focused on the mesoporous photoelectrodes with a small and narrow range of pore diameters. The relation between η and mesoporous TiO_2 pore diameter size has also not well been elucidated. Because the dye adsorption and redox shuffle electrolyte percolation are mainly determined by the pore diameter size, the conversion efficiency of DSSCs is greatly affected by the pore size of the mesoporous TiO_2 electrode. Therefore, it is of practical importance to investigate the photoelectrical conversion performance of DSSCs with a large pore diameter ($>$ 6 nm based on meso-TiO_2) and specify the relationship between η and different pore diameter sizes.

In this work, DSSCs based on meso-TiO_2 with controllable pore diameters (6.5, 8.2 and 11.0 nm) have been fabricated. The DSSC based on the 8.2 nm meso-TiO_2 photoelectrode exhibits the highest conversion efficiency, which is higher than that of conventional P25 nanoparticulate DSSCs under the same conditions. This is because it has a larger surface area and the fastest interfacial charge transfer, which is proved by N_2 sorption isotherms and photovoltage transient measurements. Meanwhile, the effect of different pore sizes on the photoelectrical conversion efficiency will be discussed in detail.

Results and Discussion

Structural Characterisation of meso-TiO_2

X-ray powder diffraction (XRD) patterns of meso-TiO_2 with controllable pore diameters (S1, S2 and S3), at different sintering temperatures, are shown in Figure 1. All the samples exhibit characteristic peaks at $2\theta \approx 25.2°$, 37.7°, 48.0°, 53.8°, 55.0° and 62.7° corresponding to the (101), (004), (200), (105), (211) and (204) plane of anatase TiO_2 (JCPDS No. 21-1272), respectively. After being annealed at 450 °C, the samples also exhibit the anatase phase, although no rutile and brookite TiO_2 can be observed. The average grain size of anatase nanocrystals was estimated by using Debye–Scherrer's equation to be in the range of 8–10 nm from the line broadening of the [101] diffraction peak.

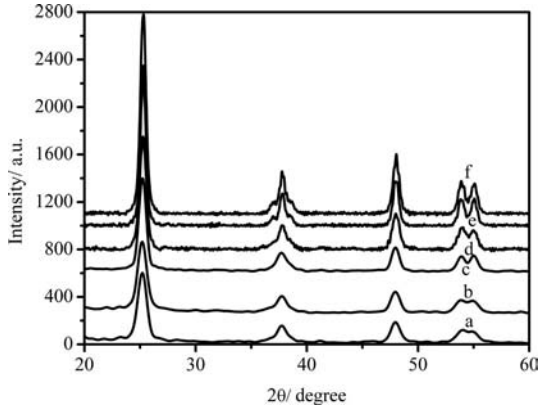

Figure 1. XRD patterns of meso-TiO_2 samples of S1 (a), S2 (b) S3 (c), S1-450 (d), S2-450 (e) and S3-450 (f), respectively.

Figure 2 depicts the N_2 sorption isotherm and pore diameter distribution of meso-TiO_2. The isotherm exhibits a type IV pattern with a hysteresis loop, which is a typical characteristic of mesoporous materials with a narrow pore-size distribution according to the IUPAC classification.[24] This type of hysteresis loop is usually related to capillary condensation and desorption in open-ended cylindrical mesopores.[25,26] The surface area of meso-TiO_2 was calculated by using the BET method, and the pore size was estimated by using the adsorption branch of the isotherm and the Barrett–Joyner–Halenda (BJH) model. The corresponding mean pore sizes were calculated to be 8.3, 10.2 and 14.0 nm for the samples S1, S2 and S3, respectively. The surface areas of S1, S2 and S3 were found to be 149, 133 and 112 $m^2 g^{-1}$, respectively (Figure S1). After the samples were sintered at 450 °C, the corresponding mean pore sizes were calculated to be 6.5, 8.2 and 11.0 nm for the samples S1-450, S2-450 and S3-450, respectively. The surface areas of S1-450, S2-450 and S3-450 were found to be 135, 117 and 93 $m^2 g^{-1}$, respectively.

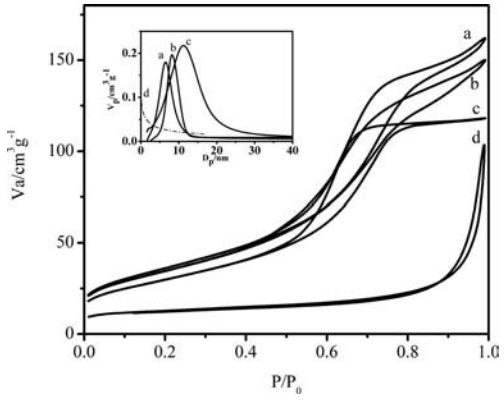

Figure 2. Nitrogen sorption isotherms of meso-TiO_2 samples of S1-450 (a), S2-450 (b), S3-450 (c) and P25 powder (d). In the inset are the corresponding Barrett-Joyner-Halenda (BJH) pore size distribution curves.

The P25 nanoparticulate powder does not possess the mesoporous structure, and its surface area is 50 $m^2 g^{-1}$. It can be noted that, although a higher annealing temperature reduces the surface area and pore size, the surface area of meso-TiO_2 is larger than that of P25 nanoparticulate powder. The results of a nitrogen adsorption/desorption experiment indicate that meso-TiO_2 has a large specific surface, and the mesopore diameter can be well controlled simply by adjusting the amount of Ti(O*n*Bu)$_4$.

Electron microscopy images and small-angle XRD patterns were used to analyse the typical meso-TiO_2 (S2) synthesised with different annealing temperatures in order to understand the features of the obtained meso-TiO_2. One can clearly see from the transmission electron microscopy (TEM) image [Figure 3(a)] that meso-TiO_2 with 350 °C an-

nealing (S2) exhibits a 2D hexagonal structure, which possesses well-ordered mesopores of about 10 nm in diameter. Figure 3(b) shows the small-angle XRD patterns of a meso-TiO_2 sample with a different annealing temperature. A sharp peak at 0.3–0.4° for S2 and S2-450 can be observed which indicates the d_{100} of the mesostructure. There are also two relatively weak peaks at around 0.5–0.7°. These results suggest the prepared meso-TiO_2 can possess a highly organised mesoporous structure when the temperature is up to 350 and 450 °C. However, the well-organised mesopores collapse thoroughly when the calcination temperature is raised to 550 °C, because no diffraction peaks can be observed from S2-550. Although the mesopore size undergoes some decrease upon higher calcination temperatures (450 °C), S2-450 still possesses a 2D ordered mesoporous structure [Figure 3(c)], which is in good agreement with the results of small-angle XRD patterns. Figure 3(d) shows the scanning electron microscopy (SEM) image of meso-TiO_2 (S2-450); meso-TiO_2 is composed of large irregularly shaped particles formed due to aggregation of several spherical nanograins. Meanwhile, the subsequent heat treatment at 450 °C results in improving the inter-particle contacts, which could enhance the transport of photoelectrons to the out-circuit and therefore favour a firm contact between the meso-TiO_2 film and the transparent conducting glass (TCO) substrate. Thus, through a facile evaporation-induced self-assembly (EISA) route, meso-TiO_2 with controllable pore size has indeed been obtained.

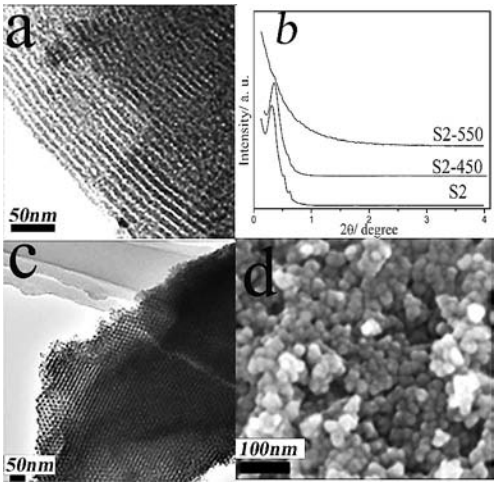

Figure 3. Typical TEM of S2 (a), small-angle XRD of S2 with different calcination temperatures (b), TEM (c) and SEM (d) image of meso-TiO_2 (S2-450) with a pore diameter of 8.2 nm

Surface Photovoltage Spectra (SPS) of meso-TiO_2

The surface photovoltage is a well-established contactless parameter for semiconductor characterisation, and this can be measured by an illumination-induced change of the surface voltage.

SPS provides detailed information about the separation capability of photo-generated electrons and holes, i.e. the band gap of the semiconductor for the sample surface layer (several atomic layers).[27] Figure 4 shows the SPS of synthesised meso-TiO_2 powders (S1-450, S2-450 and S3-450). We found the photovoltage response peaks at a wavelength of ca. 346 nm, which can be attributed to the band-band transition of anatase TiO_2. This characterisation indicates that meso-TiO_2 powders are photoelectrical material candidates for DSSC photoelectrodes.

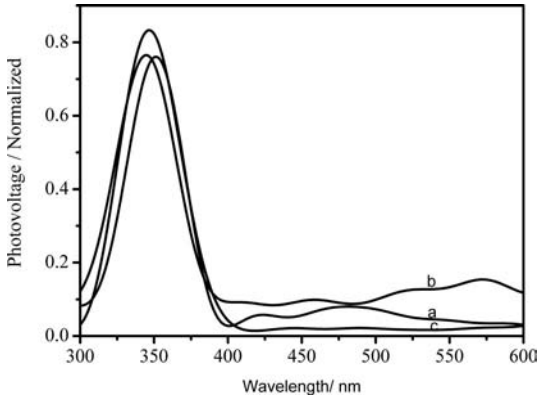

Figure 4. SPS of meso-TiO_2 nanoparticles with pore diameters of 6.2 nm (a), 8.5 nm (b) and 11.0 nm (c).

Photoelectrical Character of DSSCs with meso-TiO_2 Photoelectrodes

It is essential for meso-TiO_2 to have a large surface area and appropriate pore size to achieve high-efficiency DSSCs. If the photoelectron transfer and recombination are the same, a large surface area provides more sites to load a large amount of dye molecules, which then gives rise to higher short-circuit current densities upon light harvesting. A dye loading/unloading measurement (Figure S2) is carried out to determine the dye adsorption amount. According to the Beer–Lambert law, the molar concentration of dye unloading from E1′, E2′, E3′ and E4′ (for label definitions, see Experimental Section) is 1.6×10^{-7}, 1.5×10^{-7}, 1.3×10^{-7} and 1.0×10^{-7} mol cm^{-2}, respectively. This is consistent with surface area data of mesoporous photoelectrodes calcined at 450 °C. The appropriate pore size formed in the meso-TiO_2 photoelectrode not only provides excellent mutual connectivity for the efficient diffusion of ions in the electrolyte but also inhibits the photogenerated electron recombination with the redox shuttle electrolyte when electrons are transferred throughout the out-circuit.

In order to investigate the relationship between the η value and the different pore sizes along with the surface area, the DSSC prototype devices were fabricated by using N719-sensitised E1, E2, E3 and P25 electrodes. The photocurrent/photovoltage curves of C1, C2, C3 and C4 are shown in Figure 5. Regarding the fabrication of the cells in a convenient and reproducible way, a TiO_2 layer of 5 μm

was used. The TiO_2 films were shared with the same batch. Each value for cell performance was determined as an average of the results from at least 3 samples, and the light illumination intensity was 100 mW cm^{-2}. The values of the open-circuit voltage (V_{oc}), short-circuit current (J_{sc}), fill factor (*FF*) and overall conversion efficiency (η), obtained from the curves of solar cells, are shown in Table 1; C1 and C2 based on meso-TiO_2 with 6.5 and 8.2 nm pore sizes have η values of 5.51 and 5.81%, respectively, which are larger than that of C4 based on the conventional P25 nanoparticulate photoelectrode (5.44%), which we had prepared previously under the same conditions.[28] In contrast, C3 shows a smaller η value of 4.31%. This material was fabricated by using meso-TiO_2 with the larger mesopore size of 11.0 nm. The open-circuit voltage was determined by photoelectron recombination with the I_3^-/I^- redox shuttle electrolyte (K_{et}); C2 has the proper mesopore size, which can assure a smaller K_{et} value; C1 has a smaller pore size that makes electrolyte diffusion difficult, the excited dye cannot be recovered by the redox shuttle electrolyte effectively, and so the K_{et} value is larger; C3 has the larger pore size that makes electrolyte diffusion easy, the photoelectron recombination with the I_3^-/I^- redox shuttle electrolyte (K_{et}) is also higher. Hence, C2 has open-circuit voltages higher than C1 and C3; C4 made with the P25 nanoparticulate photoelectrode does not possess the ordered mesoporous structure, which causes the slowest photoelectron recombination rate, and so it has the highest open-circuit voltage. This demonstrates that the pore size of meso-TiO_2 plays a significant role in determining the conversion efficiency of DSSCs. The choice of meso-TiO_2 with a proper pore size can effectively improve the performance of DSSCs. After optimisation of the TiO_2 layer, the conversion efficiency could be further improved. The photocurrent/photovoltage curves of C1′, C2′, C3′ and C4′ are also shown in Figure 5. The utilised TiO_2 layer thickness was 10 μm, and the light illumination intensity was 100 mW cm^{-2}; C2′ has the highest η value of 6.50%.

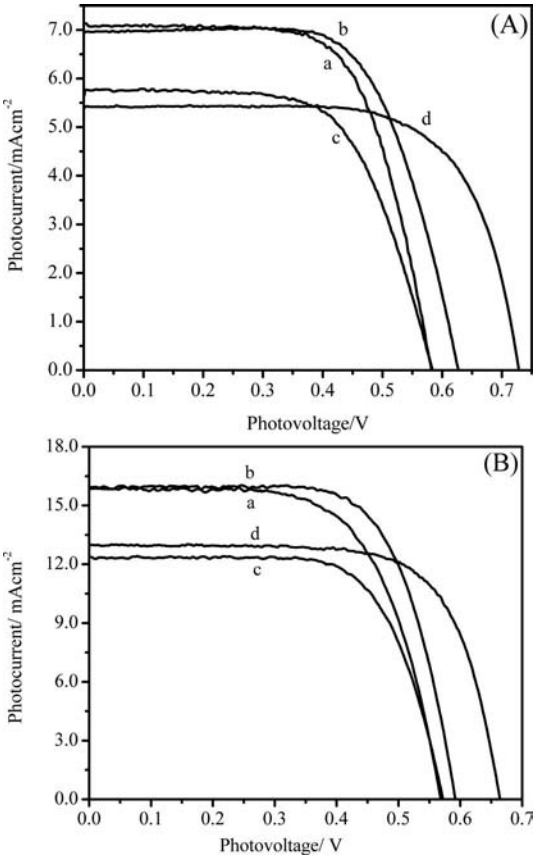

Figure 5. (A) Photocurrent/photovoltage curves of C1 (a), C2 (b), C3 (c) and C4 (d) at a light intensity of 50 mW cm^{-2}; (B) photocurrent/photovoltage curves of C1′ (a), C2′ (b), C3′ (c) and C4′ (d) ata light intensity of 100 mW cm^{-2}, respectively.

It is well known that dye adsorption and photoelectron transfer, as main factors of the photoelectrode character, determine the performance of DSSCs when other cell components are the same.[29] More dye adsorption and faster photoelectron transfer will result in a higher photoelectrical power conversion efficiency. Along with the increase in the mesopore size, the surface area of meso-TiO_2 decreases, and this does not favour a high η value. However, the decrease of mesopore size in meso-TiO_2 leads to a limited space that could hamper the redox shuffle electrolyte percolation in the photoelectrode. This will lower the oxidised dyes' recovery rate and reduce the interfacial charge transfer. Therefore, we should seek out an optimal pore size for meso-TiO_2 that ensures both a large surface area and a large space for the oxidised dyes' recovery, so as to maximise the power conversion efficiency of the cell. Our results show that C2, which applies meso-TiO_2 with a pore size of 8.2 nm, achieves the largest η value among the three investigated cells. Therefore, the pore size of 8.2 nm falls well within the size range for meso-TiO_2 to allow for a high performance of

Table 1. Solar cell parameters of C1, C2, C3, C4, C1′, C2′, C3′ and C4′, respectively.[a]

DSSC sample	Mesopore size [nm]	Surface area [m^2 g^{-1}]/thickness [μm]	J_{sc} [mA cm^{-2}]	V_{oc} [V]	*FF*	η [%]
C1	6.5	135/5	7.10	0.58	0.67	5.51
C2	8.2	117/5	7.00	0.63	0.66	5.81
C3	11.0	93/5	5.76	0.58	0.64	4.31
C4	–[b]	50/5	5.41	0.73	0.69	5.44
C1′	6.5	135/10	15.8	0.57	0.65	5.85
C2′	8.2	117/10	15.9	0.59	0.69	6.50
C3′	11.0	93/10	12.3	0.57	0.68	4.76
C4′	–[b]	50/10	13.0	0.66	0.68	5.83

[a] J_{sc}: short-circuit photocurrent; V_{oc}: open-circuit photovoltage; *FF*: fill factor; η: power conversion efficiency. [b] P25 powder is not mesoporous.

the DSSC. In the following, the interfacial charge transfer is further investigated and discussed by the photovoltage transient.

Interfacial Charge Transfer Studied by Using the Photovoltage Transient

Photovoltage-transient measurements offer direct information about the electron collection efficiency and the interfacial charge recombination.[30] An electron/hole pair is generated upon laser illumination. The photogenerated electrons traverse to the TCO, and photovoltage is obtained when the electron/hole pair separates. It has been established that the longer the distance photogenerated electrons traverse, the higher the photovoltage.[31] The whole photovoltage transient consists of the forward edge and the decay process. From the forward edge, we can obtain the separation rate of the electron/hole pair and the time when the separation distance reaches the maximum, which scales the electron-collection efficiency quantitatively. The decay process reflects the recombination rate of the electron/hole pair.

Figure 6 illustrates the photovoltage transient of DSSCs with TiO_2 electrodes of different mesopore size. All the curves are normalised, because the absolute photovoltage-transient values are not crucial for the rise time and the interfacial charge recombination. The rise time was determined to be 1.32 ms for C2, and 1.29 and 1.20 ms for C1 and C3, respectively. An increase in the uprising time indicates that C2 has a better electron-collection efficiency than the other two cells, i.e. photogenerated electrons from the excited dye move relatively long distances in C2. This is because C2 provides the proper channel for redox shuttle percolation leading to the longest travelling distance of the photogenerated electrons among the three investigated cells.

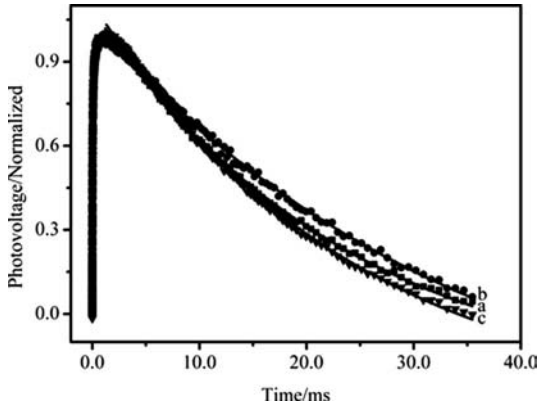

Figure 6. Photovoltage transients of C1 (a), C2 (b) and C3 (c), respectively.

The photovoltage decay involves the electron/hole pair recombination process. When the electrons are injected into the conduction band of meso-TiO_2 from the excited dye, they will recombine either with the redox shuttle or the surface traps of meso-TiO_2. The number (N) of recombined electrons per unit time is directly proportional to the number of electrons in the conduction band of meso-TiO_2:

$$\frac{dN}{dt} = -AN \quad (1)$$

A is the Einstein decay coefficient. After integration, we obtain

$$N = N_0 e^{-At} \quad (2)$$

N_0 is the photogenerated electron number before decay. When $\tau_s = 1/A$, which is defined as decay lifetime, then

$$N = N_0 e^{-t/\tau_s} \quad (3)$$

When $t = \tau_s$

$$N = N_0 e^{-t/\tau_s} \quad (4)$$

One can see that the decay of all of the photovoltage transients could be well fitted by a single exponential function, which proves that the recombination of the photoelectron with the redox shuttle or the surface traps of meso-TiO_2 is a simple process. The present investigation indicates lifetimes of 24.5, 34.8 and 24.3 ms for C1, C2 and C3, respectively. It suggests that C2 can decrease the interfacial charge recombination compared with C1 and C3. From the above photovoltage-transient data, we found that the DSSC with the pore size of 8.2 nm has the fastest interfacial charge transfer. Hence, C2 has the highest power-conversion efficiency, and this is due to higher dye adsorption, and the slowest interfacial charge recombination. Although C3 has a smaller surface area and a faster interfacial charge recombination, it exhibits a lower efficiency.

Possible Model for the Electrolyte Diffusion in the Dye-Sensitised Mesoporous Photoelectrode

Based on the above discussion, we will consider how a large pore size is most suitable for the redox shuttle electrolyte percolation in the nanochannels of the dye-sensitised mesoporous photoelectrodes. Cyclic voltammograms for mesoporous DSSCs of C1 (a), C2 (b) and C3 (c) were obtained (Figure S3). It can be clearly seen that C3 has the largest limit current, C2 has a lower one and C1 has the lowest of all. As depicted in Scheme 1, a possible model can be proposed for the electrolyte diffusion in the nanochannels of dye-sensitised mesoporous photoelectrodes. Compared with conventional np-TiO_2, meso-TiO_2 has numerous uniform nanochannels in sizes of 6.5, 8.2 and 11.0 nm for C1′, C2′ and C3′, respectively. If the adsorbed dye forms a monolayer on the inner surfaces of the nanochannels and the used N719 molecule occupies approximately 1.25 nm in space,[32] only 4, 5.7 and 8.5 nm, respectively, of space is left in the nanochannels for electrolyte diffusion after the monolayer dye coating on the inner nanochannels. If the N719 molecules adsorb in the inner surface of the channels as a bilayer or aggregate in the entrances of the nanochannels in some cases, the space for electrolyte diffusion will be reduced further. It would prohibit more dye adsorption on the inner surfaces of the nanochannels if the mesopores are not large enough. Hence, part of the inner surface could

not be covered by N719 molecules and the electrode film cannot be used efficiently. However, if the mesopore size is so large as to exceed the space needed for the redox shuttle percolation, the photoelectron recombination would become deteriorative. Therefore, a proper mesopore size is important for high-efficiency DSSCs. From the present studies of photoelectrical conversion and photovoltage data mentioned above, it can be concluded that a mesopore size of 8.2 nm is appropriate, where 5.7 nm is left for electrolyte diffusion, because C2 has the largest η value among the three investigated cells.

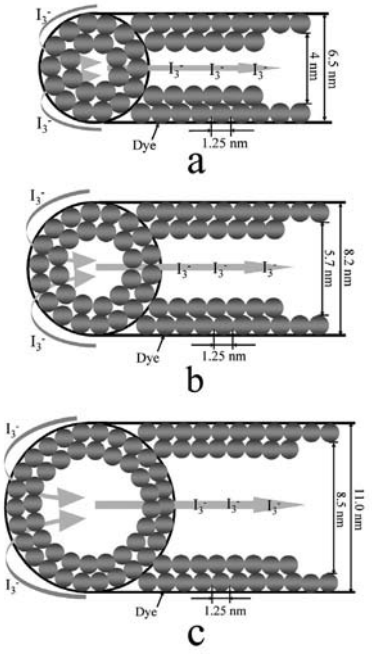

Scheme 1. Possible model for the electrolyte diffusion in the dye-sensitised mesoporous photoelectrode with pore diameters of 6.5 nm (a), 8.2 nm (b) and 11.0 nm (c), respectively.

Conclusions

In the present work, the efficiency of DSSCs has been greatly improved by using meso-TiO_2 photoelectrodes with a properly selected pore size. The pore size of meso-TiO_2 has been demonstrated to have a critical effect on the conversion efficiency of DSSCs; C2 fabricated by the TiO_2 photoelectrode with a mesopore size of 8.2 nm achieved the highest η value of 5.81%, higher than those of C1 (5.51% with 6.5 nm pores), C3 (4.31% with 11.0 nm pores) and C4 (5.44% with P25 nanoparticles). Such an improved conversion efficiency of DSSCs (with 8.2 nm meso-TiO_2) has been ascribed to the large surface area (117 $m^2 g^{-1}$), the best electron-collection efficiency (1.32 ms) and a long decay lifetime (34.8 ms), as evidenced by the measurement of N_2 sorption isotherms and the photovoltage transient. After optimisation of the TiO_2 layer to 10 μm, the conversion efficiency is improved further.

Experimental Section

Chemicals: Triblock copolymer Pluronic P123 [poly(ethylen glycol)-block-poly(propylene glycol)-block-poly(ethylene glycol), MW = 5800] and tetrabutyl titanate [Ti(O*n*Bu)$_4$] were purchased from Aldrich. The transparent conducting glass (TCO, F-doped SnO_2 layer, sheet resistance 20 Ω square^{-1}) was used as received for the electrode substrate. The Ru complex dye used was bis(tetrabutylammonium) *cis*-bis(isothiocyanato)bis(2,2′-bipyridyl-4,4′-dicarboxylato)ruthenium(II) (N719, Solaronix SA). The redox shuttle electrolyte was composed of 0.1 M LiI (anhydrous, 99%, Acros), 0.05 M I_2 (≥ 99.8%), 0.5 M 4-*tert*-butylpyridine (99%, Aldrich) and 0.6 M 1-propyl-2,3-dimethylimidazolium iodide (99%) in 3-methoxypropionitrile (99%, Fluka). Ultrapure water (18 MΩ cm) was used during the whole experimental process. All the other solvents and chemicals used in the experiments are at least reagent grade and were used as received.

Synthesis of meso-TiO_2 with Controllable Pore Diameters: The large-pore meso-TiO_2 was synthesised by the evaporation-induced self-assembly (EISA) method, which is similar to that in our previous report.[33,34] Generally, 10 M HCl was slowly added to Ti(O*n*Bu)$_4$ under vigorous stirring at room temperature. A solution of P123 dissolved in ethanol was then added, followed by further stirring for 2 h. The typical weights in grams of each reactant were Ti(O*n*Bu)$_4$/HCl/P123/EtOH = *x*:3.2:1:12, where *x* is 2.6, 2.7 and 3.4. After the resultant sols were aged at room temperature with 50–60% relative humidity for 24 h, they were then calcined at 350 °C (ramp of 1 °C min^{-1}) in air for 4 h to remove the block copolymer surfactant. The large pore size of meso-TiO_2 could be tailored by simply adjusting the amounts of Ti(O*n*Bu)$_4$. The obtained meso-TiO_2 samples with pore diameters of 8.3, 10.2 and 14 nm were labelled as S1, S2 and S3, respectively. The samples of S1, S2 and S3 were then calcined at 450 °C (ramp of 1 °C min^{-1}) for 30 min in order to obtain better crystallinity, and they were labelled as S1-450, S2-450 and S3-450, respectively. The sample S2-450 calcined at 550 °C (ramp of 1 °C min^{-1}) was labelled as S2-550.

Dye-Sensitised meso-TiO_2 Photoelectrode Fabrication and DSSCs Assembly: The compositions of three kinds of mesoporous TiO_2 paste with S1-450, S2-450 and S3-450 were as follows: 1 g of mesoporous TiO_2 powder, 2 mL of distilled water, 5 drops of Triton X-100 and 2 drops of acetylacetone. A doctor-blade technique was used to fabricate the photoelectrodes on a TCO substrate. A thin film was obtained by using a glass rod to scrape off the excessive paste. After being air-dried for 30 min, they were sintered at 450 °C (ramping rate 1 °C min^{-1}) for 30 min. Repetitive coating was carried out as the first electrodes cooled down to room temperature by repeating the above procedure. All film electrodes were fabricated with two different thicknesses (5 μm and 10 μm) as determined by SEM images. The available photoelectrodes of 5 μm thickness with S1-450, S2-450 and S3-450 were labelled as E1, E2 and E3, respectively. The available photoelectrodes of 10 μm thickness with S1-450, S2-450 and S3-450 were labelled as E1′, E2′ and E3′, respectively. As a control, the P25 electrode was also prepared according to the conventional method,[35] and the P25 photoelectrodes with a thickness of 5 μm or 10 μm were labeled as E4 and E4′, respectively. These meso-TiO_2 photoelectrodes were sensitised by immersing in 0.5 mM N719 dye solution for 48 h so that the dye could be adsorbed onto the surface of the TiO_2 electrodes sufficiently. The counter electrode was prepared according to previous work.[36] The dye-sensitised E1, E2, E3 and E1′, E2′, E3′ with a Pt counter electrode were adhered together with epoxy resin. The space between the electrodes was filled with the electrolyte by capillary action.

The fabricated DSSCs based on photoelectrodes of E1, E2, E3 and E1′, E2′, E3′ were labelled as C1, C2, C3 and C1′, C2′, C3′, respectively. The DSSCs based on E4 and E4′ were also fabricated according to the common method[35] and labelled as C4 and C4′, respectively.

Characterisation: XRD patterns were obtained by using a Rigaku D/max-IIIB diffractometer with Cu-K_α radiation (λ = 1.5406 Å). The nitrogen adsorption/desorption isotherms were measured by using a TriStar II 3020 instrument at 77 K. The TEM experiment was performed with a JEM-3010 electron microscope (JEOL, Japan) ba using an acceleration voltage of 200 kV. Carbon-coated copper grids were used as the sample holders. SEM images were taken with a Hitachi S-4800 instrument operating at 15 kV. The surface photovoltage spectra (SPS) were carried out with a laboratory-built surface photovoltage spectrometer. A 150 W xenon lamp with a monochromator was used as the light source. The illumination direction was from the TiO_2 electrode. The generation of a photovoltage arose from the creation of electron/hole pairs followed by the separation under a built-in electric field (the space-charge layer). The dye-sensitised photoelectrodes were desorbed in a 0.02 M NaOH solution in alcohol (EtOH)/H_2O (1:1, v/v) for 6 h to measure the adsorption dye amount. Photocurrent/photovoltage curves were recorded with a BAS100B electrochemical analyser (Bioanalytical Systems Inc., USA). A 400 W xenon lamp with a UV filter was used as the light source. Its illumination intensity was about 50 mW cm^{-2} for DSSCs with a 5 μm mesoporous photoelectrode and 100 mW cm^{-2} for DSSCs with a 10 μm mesoporous photoelectrode. The area of the DSSCs was 1.5 cm^2. With the mask, the irradiation area was 0.12 cm^2. The photovoltage transient measurements were recorded with a TDS 5054 Digital Phosphor Oscilloscope (Tektronix, USA). A Polaris II Nd:YAG laser (New Wave Research Inc., USA) was used to excite the samples C1, C2 and C3. The 532 nm wavelength of the laser was selected because the N719 dye has the maximum absorption at about 512 nm, and the average energy of each laser pulse was about 100 μJ with a standard deviation of 20 μJ. The photovoltage transient measurement was carried out under open-circuit conditions, and the incident light was from the photoelectrode side of the DSSCs. The setup scheme, the principles of SPS and the photovoltage transient are shown in our previous work.[37] Cyclic voltammetry (CV) was performed with the BAS100B electrochemical analyser (Bioanalytical Systems Inc., USA) with a scan rate of 0.1 V S^{-1}.

Supporting Information (see footnote on the first page of this article): Nitrogen sorption isotherms of meso-TiO_2 samples of S1, S2 and S3 with the corresponding Barrett-Joyner-Halenda (BJH) pore-size distribution curves; absorption spectra of N719 dye unloading from C1′, C2′, C3′ and C4′, respectively; cyclic voltammograms for mesoporous DSSCs of C1, C2 and C3, respectively.

Acknowledgments

We gratefully acknowledge the support of this research by the Key Program Projects of the National Natural Science Foundation of China (21031001), the National Natural Science Foundation of China (20971040, 21001042, 20703015), the Cultivation Fund of the Key Scientific and Technical Innovation Project, Ministry of Education of China (708029), the Program for New Century Excellent Talents in Heilongjiang Provincial University of China (1154-NCET-010), the Excellent Youth of Common Universities of Heilongjiang Province of China (1154G24), the Harbin Youth Foundation (2009RFQXG202), and the Scientific Research Fund of Heilongjiang Provincial Education Department (11541283, 12511376).

[1] B. O'Regan, M. Grätzel, *Nature* **1991**, *353*, 737–739.
[2] M. K. Nazeeruddin, A. Kay, I. Rodicicio, R. Humphry-Baker, E. Muller, P. Liska, N. Vlachopoulos, M. Grätzel, *J. Am. Chem. Soc.* **1993**, *115*, 6382–6390.
[3] U. Bach, D. Lupo, P. Comte, J. E. Moser, F. Weissortel, J. Salbeck, H. Spreitzer, M. Grätzel, *Nature* **1998**, *395*, 583–585.
[4] A. Petrozza, C. Groves, H. J. Snaith, *J. Am. Chem. Soc.* **2008**, *130*, 12912–12910.
[5] A. Hagfeldt, M. Grätzel, *Chem. Rev.* **1995**, *95*, 49–68.
[6] S. A. Haque, E. Palomares, B. M. Cho, A. N. M. Green, N. Hirata, D. R. Klug, J. R. Durrant, *J. Am. Chem. Soc.* **2005**, *127*, 3456–3462.
[7] J. R. Durrant, S. A. Haque, E. Palomares, *Coord. Chem. Rev.* **2004**, *248*, 1247–1257.
[8] A. B. F. Martinson, T. W. Hamann, M. J. Pellin, J. T. Hupp, *Chem. Eur. J.* **2008**, *14*, 4458–4467.
[9] M. Grätzel, *J. Photochem. Photobiol. C: Photochem. Rev.* **2003**, *4*, 145–153.
[10] M. Grätzel, *J. Photochem. Photobiol. A: Chem.* **2004**, *164*, 3–14.
[11] L. M. Peter, *J. Phys. Chem. C* **2007**, *111*, 6601–6612.
[12] B. C. O'Regan, K. Bakker, J. Kroeze, H. Smit, P. Sommeling, J. R. Durrant, *J. Phys. Chem. B* **2006**, *110*, 17155–17160.
[13] M. Adachi, Y. Murata, J. Takao, J. Jiu, M. Sakamoto, F. Wang, *J. Am. Chem. Soc.* **2004**, *126*, 14943–14949.
[14] E. Palomares, J. N. Clifford, S. A. Haque, T. Lutz, J. R. Duarrant, *J. Am. Chem. Soc.* **2003**, *125*, 475–482.
[15] C. L. Clement, R. T. Zaera, M. A. Ryan, A. Katty, G. Hodes, *Adv. Mater.* **2005**, *17*, 1512–1515.
[16] M. Law, L. E. Greene, J. C. Johnson, R. Saykally, P. Yang, *Nat. Mater.* **2005**, *4*, 455–459.
[17] M. Law, L. E. Greene, A. Radenovic, T. Kuykendall, J. Liphardt, P. Yang, *J. Phys. Chem. B* **2006**, *110*, 22652–22663.
[18] M. Grätzel, *Curr. Opin. Colloid Interface Sci.* **1999**, *4*, 314–321.
[19] I. Kartini, D. Menzies, D. Blake, J. C. D. da Costa, P. Meredith, J. D. Riches, G. Q. Lu, *J. Mater. Chem.* **2004**, *14*, 2917–2921.
[20] K. Hou, B. Tian, F. Li, Z. Bian, D. Zhao, C. Huang, *J. Mater. Chem.* **2005**, *15*, 2414–2420.
[21] M. Wei, Y. Konishi, H. Zhou, M. Yanagida, H. Sugihara, H. Arakawa, *J. Mater. Chem.* **2006**, *16*, 1287–1293.
[22] N. Alexaki, T. Stergiopoulos, A. G. Kontos, D. S. Tsoukleris, A. P. Katsoulidis, P. J. Pomonis, D. J. LeClere, P. Skeldon, G. E. Thompson, P. Falaras, *Microporous Mesoporous Mater.* **2009**, *124*, 52–58.
[23] S. R. Gajjela, K. Ananthanarayanan, C. Yap, M. Grätzel, P. Balaya, *Energy Environ. Sci.* **2010**, *3*, 838–845.
[24] S. J. Gregg, K. S. W. Sing in *Adsorption, Surface Area and Porosity*, Academic Press, London, **1982**.
[25] S. A. El-Safty, T. Hanaoka, F. Mizukami, *Adv. Mater.* **2005**, *17*, 47–53.
[26] M. Kruk, M. Jaroniec, C. H. Ko, R. Ryoo, *Chem. Mater.* **2000**, *12*, 1961–1968.
[27] Y. Lin, D. Wang, Q. Zhao, M. Yang, Q. Zhang, *J. Phys. Chem. C* **2004**, *108*, 3202–3206.
[28] K. Pan, Y. Z. Dong, C. G. Tian, W. Zhou, G. H. Tian, B. F. Zhao, H. G. Fu, *Electrochim. Acta* **2009**, *54*, 7350–7356.
[29] F. Sauvage, F. Di Fonzo, A. L. Bassi, C. S. Casari, V. Russo, G. Divitini, C. Ducati, C. E. Bottani, P. Comte, M. Grätzel, *Nano Lett.* **2010**, *10*, 2562–2567.
[30] X. Wei, T. Xie, D. Xu, Q. Zhao, S. Pang, D. Wang, *Nanotechnology* **2008**, *19*, 275707.
[31] Y. Dong, K. Pan, W. Zhou, Q. Pan, T. Xie, D. Wang, H. Fu, *Dalton Trans.* **2011**, *40*, 3808–3814.
[32] V. Shklover, Y. E. Ovchinnikov, L. S. Braginsky, S. M. Zakeeruddin, M. Grätzel, *Chem. Mater.* **1998**, *10*, 2533–2541.
[33] K. S. Liu, H. G. Fu, K. Y. Shi, F. S. Xiao, L. Q. Jing, B. F. Xin, *J. Phys. Chem. B* **2005**, *109*, 18719–18722.

[34] W. Zhou, H. G. Fu, K. Pan, C. G. Tian, Y. Qu, P. P. Lu, C. C. Sun, *J. Phys. Chem. C* **2008**, *112*, 19584–19589.
[35] C. J. Barbé, F. Arendse, P. Comte, M. Jirousek, F. Lenzmann, V. Shklover, M. Grätzel, *J. Am. Ceram. Soc.* **1997**, *80*, 3157–3171.
[36] A. Hagfeldt, M. Grätzel, *Acc. Chem. Res.* **2000**, *33*, 269–277.
[37] K. Pan, Q. L. Zhang, Q. Wang, Z. Y. Liu, D. J. Wang, J. H. Li, Y. B. Bai, *Thin Solid Films* **2007**, *515*, 4085–4091.

Received: April 12, 2011
Published Online: September 8, 2011

